Malaysian Journal of Mathematical Sciences

Journal homepage: https://einspem.upm.edu.my/journal

Entropy Generation in Casson Nanofluid Flow Past an Electromagnetic Stretching Riga Plate

Oyelakin, I.S.[1], Ghosh, R.[2], Mondal, S.[2,*], and Sibanda, P. [3]

[1]*School of Computer Science and Applied Mathematics, University of the Witwatersrand, South Africa*
[2]*Department of Mathematics, Amity University, India*
[3]*School of Mathematics, Statistics and Computer Science, University of KwaZulu-Natal, South Africa*

Email: sabya.mondal.2007@gmail.com
**Correponding author*

Received: 23 September 2019
Accepted: 26 April 2021

Abstract

This paper investigates entropy generation in a Casson nanofluid flow past an electromagnetic stretching Riga plate. Entropy generation is a measure of irreversibility factors in thermodynamic processes. It is a common feature in heat transfer studies, and as such, the study includes the effect of viscous dissipation. We solve the model equations using the spectral local linearization method. The study considers the impact of some other physical parameters like the Casson, velocity ratio, and electromagnetic parameters. A good correlation is achieved when the present results are compared with published literature. The results indicate that the velocity ratio parameter significantly influences the fluid flow, temperature, and concentration profiles. The entropy generation increases with an increase in concentration and Brinkmann number, whereas an opposite behavior is observed for increasing the value of the modified Hartmann number. Again, increasing the Casson parameter increases the temperature and concentration profiles, whereas the velocity profile reduces.

Keywords: entropy generation; Riga plate; Casson nanofluid; spectral local linearization method.

1 Introduction

Choi [8] introduced the concept of nanofluids. In his pioneer work on nanofluids, he proposed that nanoparticles be suspended in a certain base fluid such as oil, water, kerosene, and ethylene glycol. A nanofluid is a fluid that contains a suspension of nanoparticles. It is assumed that the nanoparticles are uniformly and stably distributed in a base fluid. Das et al. [10] pointed out some unique nanofluid features. These are the abnormal enhancement of thermal conductivity, stability, and particle size dependence. Buongiorno [6] attempted to explain the increase in the thermal conductivity of nanofluids. He introduced a model that took into account the particle Brownian motion and thermophoresis diffusion. Researchers used Buongiorno's model and studied nanofluid flows with the magnetic field, thermal radiation, viscous dissipation, porosity, and stability. Noghrehabadi et al. [30] investigated the effect of partial slip(that is, the Navier's condition) on the boundary layer flow and heat transfer of nanofluids past a stretching sheet. They observed that the slip parameter strongly influences the flow velocity, and the surface shear stress on the stretching sheet. They concluded that there is a decrease in the momentum boundary layer thickness and an increase in the thermal boundary layer thickness.

Khan and Pop [18] investigated numerically the problem of laminar fluid flow, which results from the stretching of a flat surface in a nanofluid. The model they studied included the effect of Brownian motion and thermophoresis diffusion. They found that the reduced Sherwood number increased with the parameters considered in the study. Makinde et al.[22] studied the boundary layer flow in a nanofluid using a convective heating boundary condition. Their result showed that for fixed values of the Prandtl, Lewis, and Biot numbers, the local temperature rises as the Brownian motion and thermophoresis effects intensify. However, when the Prandtl number, Brownian motion, thermophoresis diffusion, and Biot number are fixed, the temperature distribution is slightly affected. Hamad [15] examined heat transfer in an incompressible viscous nanofluid flow past a semi-infinite vertical stretching sheet in the presence of a magnetic field.

Casson fluid is a non-newtonian fluid. It can be defined as a shear-thinning liquid assumed to have an infinite viscosity at zero rates of shear, yield stress below which no flow occurs, and a zero viscosity at an infinite rate of shear, Dash et al.[11]. It behaves like an elastic solid at low shear strain, and above a critical stress value, it behaves like a Newtonian fluid. Some examples of Casson fluid are tomato, honey, and human blood [26]. Recently, studies in Casson nanofluid have gained popularity. [27] carried out an analysis on Casson nanofluid flow past a non-linearly stretching sheet with magnetic field effects. They concluded that Brownian motion has a negligible impact on temperature and heat transfer rate on the sheet; also, the skin friction coefficient values for the Casson fluid are greater than those of the Newtonian fluid.

Makanda et al. [21] analyzed the diffusion of chemically reactive species in Casson fluid flow over an unsteady stretching surface. They observed that with an increase in magnetic and permeability parameters, the velocity profiles decreases, and the skin friction increases. In contrast, the rate of heat, as well as the concentration profiles, are decreased. Raju et al.[34] examined the flow, heat, and mass transfer behavior in a Casson fluid flow past an exponentially permeable stretching surface. Their study included magnetic field effects, thermal radiation, viscous dissipation, heat source, and chemical reaction. They showed that chemical reaction and magnetic field parameters tend to minimize the skin friction coefficient. Oyelakin et al.[32] studied the combined effects of Soret and Dufour numbers on the fluid flow, heat, and mass transfer of a Casson nanofluid over an unsteady stretching sheet with thermal radiation and heat generation.

Kuznetsov and Neild [20] revisited the problem of natural convective boundary layer flow of a nanofluid past a vertical plate, including the effects of Brownian motion and thermophoresis

diffusion. Their new model argued that the nanofluid particle on the boundary should be passive rather than actively controlled to have a more realistic model.

A new mechanism that produces wall-parallel Lorentz force was developed by [12]. They proposed an electromagnetic actuator, which consists of permanent magnets and electrodes scaled on a plane surface. The setup is known as Riga-plate. The advantage of such a setup is that it prevents boundary layer separation and reduces turbulence effects. Additionally, it diminishes pressure drag and friction in submarines. Mixed convection nanofluid flow bounded by a convectively heated vertical Riga-plate has been studied by [3, 4]. In contrast, [16] studied the flow of a nanofluid past a convectively heated Riga-plate with variable thickness.

Entropy generation is associated with thermodynamic irreversibility, a common feature in most heat transfer processes. [2] studied fluid flow heat and mass transfer and entropy generation in a steady Casson nanofluid flow past a stretching sheet with velocity slip and convective boundary condition. Entropy generation on MHD Casson nanofluid flow over a porous stretching/shrinking surface was studied by [33]. Their study included the influence of nonlinear thermal radiation and chemical reaction. Entropy generation on nanofluid flow through a horizontal Riga plate was investigated by [1]. Entropy generation in unsteady two-dimensional squeezing flow between two Riga-plates was studied by [5]. Their study included a Cattaneo Christov heat flux model and a convective boundary condition.

Recently, Oyelakin and Sibanda [31] examined entropy generation in a Casson nanofluid radiative flow. They assumed a thermophoretic diffusion at the solutal boundary and showed that the entropy generation number increases with increment in temperature difference. Also, the irreversibility of heat transfer is a significant source for entropy generation. Entropy generation on double-diffusive nanofluid flow with activation energy was investigated by [19]. [13][14] observed that the entropy generation diminishes by the dynamic viscosity of fluid used in the study.

The study of entropy generation in a Casson nanofluid flow past an electromagnetic stretching Riga sheet has not been given much consideration to the best of the authors' knowledge. This paper aims to study the fluid flow, heat transfer, mass transfer, and entropy generation effects in a Casson nanofluid flow on an electromagnetic sheet. The traditional Casson nanofluid model is revised to include the impact of the electromagnetic parameter. In this paper, we use the spectral local realization method proposed by Motsa [24] to solve the model equations. The spectral local linearization method has the quirk of fast convergence and good accuracy, as shown in some recent studies [35, 7]. This study has a wide application in numerous industrial disciplines such as the cooling of electronic devices, transportation, etc.

2 Mathematical Formulation

Consider a coordinate system that originates from the leading edge of the Riga-plate. In this study, we focus on the Buongiorno model, which considers the Brownian motion and thermophoresis diffusion of nanoparticles. Moreover, the influence of viscous dissipation is considered in the flow. Here, u and v are the velocity components in the x and y directions, respectively. The x-axis is assumed to be along the sheet, and the y-axis is perpendicular to it, as shown in Figure 1.

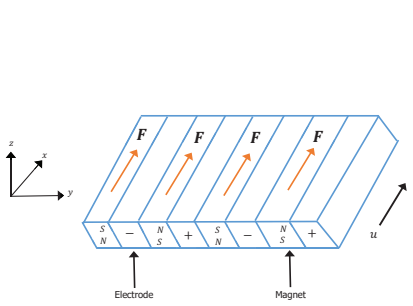

(a)An electromagnetic Riga-plate comprising an array of electrodes and permanent magnets

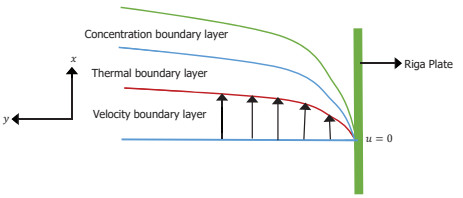

(b)Stretching sheet

Figure 1: Physical configuration and coordinate system of the problem.

A wall parallel to Lorentz force of exponentially decaying nature is created due to an electromagnetic field produced by the Riga-plate. The velocity at the ambient fluid is denoted by $u_\infty(x) = cx$, where c is a positive constant. Using the above assumptions, the boundary layer equations are [17]

$$\frac{\partial u}{\partial x} + \frac{\partial v}{\partial y} = 0, \tag{1}$$

$$u\frac{\partial u}{\partial x} + v\frac{\partial u}{\partial y} = u_\infty \frac{du_\infty}{dx} + \frac{\mu_f}{\rho_f}\left(1 + \frac{1}{\beta}\right)\frac{\partial^2 u}{\partial y^2} + \frac{\pi j_0 M_0}{8\rho_f} e^{-(\pi/\Lambda)y}, \tag{2}$$

$$u\frac{\partial T}{\partial x} + v\frac{\partial T}{\partial y} = \frac{k_f}{(\rho c_p)_f}\frac{\partial^2 T}{\partial y^2} + \tau\left[D_B\frac{\partial C}{\partial y}\frac{\partial T}{\partial y} + \frac{D_T}{T_\infty}\left(\frac{\partial T}{\partial y}\right)^2\right] + \frac{\mu_f}{(\rho c_p)_f}\left(1 + \frac{1}{\beta}\right)\left(\frac{\partial u}{\partial y}\right)^2, \tag{3}$$

$$u\frac{\partial C}{\partial x} + v\frac{\partial C}{\partial y} = D_B\frac{\partial^2 C}{\partial y^2} + \frac{D_T}{T_\infty}\frac{\partial^2 T}{\partial y^2}. \tag{4}$$

The associated boundary conditions are

$$u = u_w(x) = ax, v = 0, \quad T = T_w, C = C_w \text{ as } y = 0, \tag{5}$$

$$u \to u_\infty(x) = cx, T \to T_\infty, C \to C_\infty \text{ as } y \to \infty, \tag{6}$$

where u and v are the respective velocities along x and y directions., β is the Casson number, C and T are solutal concentration and temperature, respectively. The heat capacity of the fluid be $\tau = \varepsilon(\rho c)_p/(\rho c)_f$ with $(\rho c)_f$ and $(\rho c)_p$ are the effective heat capacity of the nanoparticle material, D_B, and D_T are the Brownian diffusion coefficient and thermophoresis diffusion coefficient, respectively, ρ is the density of the fluid, j_0 is the density of current, and M_0 is the magnetization of magnets.

To transform the partial differential equations into a system of ordinary differential equations, we introduce the following dimensionless variables

$$\psi = x\sqrt{a\nu_f}f(\eta), \quad \eta = \sqrt{\frac{a}{\nu_f}}y, \quad \theta(\eta) = \frac{T - T_\infty}{T_w - T_\infty}, \quad \phi(\eta) = \frac{C - C_\infty}{C_w - C_\infty}. \tag{7}$$

Using the stream function equations,

$$u = axf^{'}(\eta) \quad \text{and} \quad v = -\sqrt{a\nu_f}f(\eta),$$

the continuity equation in (1) is readily satisfied and the dimensionless form of equations (2) - (4) become

$$\left(1+\frac{1}{\beta}\right)f''' + ff'' - f'^2 + Ze^{-\eta\delta} + \epsilon^2 = 0, \tag{8}$$

$$\frac{1}{Pr}\theta'' + f\theta' + \left(1+\frac{1}{\beta}\right)Ecf''^2 + Nb\phi'\theta' + Nt\theta'^2 = 0, \tag{9}$$

$$\phi'' + Lef\phi' + \frac{Nt}{Nb}\theta'' = 0, \tag{10}$$

and the corresponding dimensionless boundary conditions become:

$$f(0) = 0, f^{'}(0) = 1, \theta(0) = 1, \phi(0) = 1, \tag{11}$$

$$f^{'}(\infty) \to \epsilon, \theta^{'}(\infty) \to 0, \phi^{'}(\infty) \to 0, \tag{12}$$

where $Pr = \frac{\nu_f(\rho c_p)_f}{K_f}$ is the Prandtl number, $Le = \frac{\nu_f}{D_B}$ is the Lewis number, $Nb = \frac{\tau D_B}{\nu_f}(C_w - C_\infty)$ is the Brownian motion parameter, $Nt = \frac{\tau D_T}{\nu_f T_\infty}(T_w - T_\infty)$ is the thermophoresis parameter, $\epsilon = \frac{c}{a}$ is the velocity ratio parameter, $Z = \frac{\pi M_0 j_0 x}{8\rho_f u_w^2}$ is the modified Hartmann number, $\delta = \frac{\pi}{\Lambda\sqrt{\frac{a}{\nu_f}}}$ is the width parameter, $Ec = \frac{u_w^2}{c_p(T_w - T_\infty)}$ is the local Eckert number.

The coefficient of skin friction, the local Nusselt number and the local sherwood number are given as

$$Cf_x = \frac{\tau_w}{\rho_f u_w^2}, \quad Nu_x = \frac{q_w x}{k_f(T_w - T_\infty)}, \quad Sh_x = \frac{q_m x}{D_B(C_w - C_\infty)}, \tag{13}$$

where

$$\tau_w = \left(\mu_B + \frac{p_y}{\sqrt{2\pi_c}}\right)\mu_f \left.\frac{\partial u}{\partial y}\right|_{y=0}, \quad q_w = -k_f \left.\frac{\partial T}{\partial y}\right|_{y=0}, \quad q_m = -D_B \left.\frac{\partial C}{\partial y}\right|_{y=0}. \tag{14}$$

Substituting (14) into (13), we obtain

$$Cf_x = \frac{\mu_f}{\rho_f u_w^2}\left(1+\frac{1}{\beta}\right)\left.\frac{\partial u}{\partial y}\right|_{y=0}, \quad Nu_x = -\frac{x}{(T_w - T_\infty)}\left.\frac{\partial T}{\partial y}\right|_{y=0},$$
$$Sh_x = -\frac{x}{(C_w - C_\infty)}\left.\frac{\partial C}{\partial y}\right|_{y=0}. \tag{15}$$

Next, substitute (7) into (15), to give

$$Re_x^{\frac{1}{2}} Cf_x = \left(1+\frac{1}{\beta}\right)f''(0), \quad Re_x^{-\frac{1}{2}} Nu_x = -\theta'(0),$$
$$Re_x^{-\frac{1}{2}} Sh_x = -\phi'(0), \tag{16}$$

where $Re_x = u_w x/\nu_f$ is the Reynolds number.

3 Entropy Generation Analysis

The entropy generation for the Casson nanofluid is expressed by [5]

$$S_{gen} = \frac{k_f}{T_\infty^2}\left(\frac{\partial T}{\partial y}\right)^2 + \frac{\mu_f}{T_\infty}\left(1+\frac{1}{\beta}\right)\left(\frac{\partial u}{\partial y}\right) + \frac{RD_B}{C_\infty}\left(\frac{\partial C}{\partial y}\right)^2 + \frac{RD_B}{T_\infty}\left(\frac{\partial T}{\partial y}\frac{\partial C}{\partial y}\right). \tag{17}$$

In equation (17), the first term is due to heat transfer, the second term is due to fluid friction, and the third term is due to mass transfer. The characteristic entropy generation is defined as

$$S_0 = \frac{k_f\left(T_w - T_\infty\right)^2}{T_\infty^2 x^2}. \tag{18}$$

Using the similarity transformations defined in equation (7), the entropy generation in dimensionless form is written as

$$N_G = \frac{S_{gen}}{S_0} = Re\theta'^2 + \frac{BrRe}{\Omega}\left(1+\frac{1}{\beta}\right)f''^2 + \lambda_1 Re\left(\frac{\chi}{\Omega}\right)^2\phi'^2 + \lambda_1 Re\left(\frac{\chi}{\Omega}\right)\theta'\phi', \tag{19}$$

where $Re, Br, \Omega, \lambda_1$ and χ are the Reynold's number, Brinkmann number, dimensionless temperature, diffusion coefficient and dimensionless concentration, respectively, and are defined as

$$Re = \frac{u_w x}{\nu_f},\ \ Br = \frac{\mu_f u_w^2}{k_f\left(T_w - T_\infty\right)},\ \ \Omega = \frac{\left(T_w - T_\infty\right)}{T_\infty},\ \ \lambda_1 = \frac{RD_B C_\infty}{k_f},\ \ \chi = \frac{\left(C_w - C_\infty\right)}{C_\infty}. \tag{20}$$

In irreversibility studies, a ratio of the heat transfer irreversibility to total irreversibility is termed the Bejan number and is defined as

$$Be = \frac{Re\theta'^2}{Re\theta'^2 + \frac{BrRe}{\Omega}\left(1+\frac{1}{\beta}\right)f''^2 + \lambda_1 Re\left(\frac{\chi}{\Omega}\right)^2\phi'^2 + \lambda_1 Re\left(\frac{\chi}{\Omega}\right)\theta'\phi'}. \tag{21}$$

Three cases are examined for the Bejan number: Firstly, if $Be < 0.5$, this implies that the total irreversibility dominates. Secondly, if $Be > 0.5$, this means that the heat transfer irreversibility dominates. Lastly, if $Be = 1$, this implies that the irreversibility results from the heat transfer only.

4 Method of Solution

To solve the differential equations in (8) - (10), we use the spectral local linearization method as described by [23]. Researchers have used the spectral local linearization method to solve mathematical model equations [28, 39]. The method has proved to be highly convergent with a high accuracy level. The method is described in details by [23, 37, 36]. The local linearization scheme corresponding to equations (8) - (10) is

$$a_{0,r}f'''_{r+1} + a_{1,r}f''_{r+1} + a_{2,r}f'_{r+1} + a_{3,r}f_{r+1} = R_{1,r}, \tag{22}$$
$$b_{0,r}\theta''_{r+1} + b_{1,r}\theta'_{r+1} = R_{2,r}, \tag{23}$$
$$\phi''_{r+1} + c_{1,r}\phi'_{r+1} = R_{3,r}, \tag{24}$$

where the subscript $r+1$ and r represent the current iteration and previous iterations, respectively. The variable coefficients $a_{i,r},\ b_{i,r}$ and $c_{i,r}(i = 1, 2, 3, \cdots)$ are defined as:

$$a_{0,r} = \left(1 + \frac{1}{\beta}\right), \quad a_{1,r} = f_r, \quad a_{2,r} = -2f'_r, \quad a_{3,r} = f''_r, \quad b_{0,r} = \frac{1}{Pr}, \quad b_{1,r} = f_r + Nb\phi'_r + 2Nt\theta'_r,$$
and $c_{1,r} = Lef_r$.

The right hand sides are given as

$$R_{1,r} = a_{0,r}f'''_r + a_{1,r}f''_r + a_{2,r}f'_r + a_{3,r}f_r - F_1, \tag{25}$$
$$K_{2,r} = b_{0,r}\theta''_r + b_{1,r}\theta'_r - F_2, \tag{26}$$
$$R_{3,r} = \phi''_r + c_{1,r}\phi'_r - F_3, \tag{27}$$

where

$$F_1 = \left(1 + \frac{1}{\beta}\right) f'''_r + f_r f''_r - f'^2_r + Ze^{-\eta\delta} + \epsilon^2, \tag{28}$$
$$F_2 = \frac{1}{Pr}\theta''_r + f_r\theta'_r + \left(1 + \frac{1}{\beta}\right) Ecf''^2_r + Nb\phi'_r\theta'_r + Nt\theta'^2_r, \tag{29}$$
$$F_3 = \phi''_r + Lef_r\phi'_r + \frac{Nt}{Nb}\theta''_r. \tag{30}$$

We solve the equations starting from a given set of suitable initial approximations. The semi-infinite domain $[0, \infty]$ to a truncated domain $[0, L_\infty]$, where, L_∞ is a finite number which is large enough to represent the flow conditions at ∞. $\eta \in [0, L_\infty]$ is now transformed to $x \in [-1, 1]$ using a suitable linear transformation. The Chebyshev differentiation matrix $\mathbf{D}$ as defined in [40] is introduced to estimate the derivatives of the unknown variables at the collocation points as matrix vector product represented as

$$\frac{df}{d\eta} = \sum_{j=0}^{Nx} \mathbf{D}_{jk} f(x_j) = \mathbf{D}F, \quad k = 0, 1, 2, \cdots, Nx, \tag{31}$$

where N_x+1 is the number of collocation points, $\mathbf{D} = 2D/C_\infty$ and $F = [f(x_0), f(x_1), \cdots, f(x_{Nx})]^T$ is a vector function at the collocation points. Higher order derivatives are obtained as powers of $\mathbf{D}$, that is,

$$\frac{d^s f}{d\eta^s} = \mathbf{D}^s F, \tag{32}$$

where s is the order of the derivative and the matrix $\mathbf{D}$ is of size $(N_x + 1) \times (N_x + 1)$. The Gauss-Lobatto points are chosen to define the nodes in $[-1, 1]$ as

$$x_i = \cos\frac{\pi i}{N_x}, \quad i = 0, 1, \cdots, N_x; \quad -1 \le x \le 1. \tag{33}$$

Applying (31) to the scheme in (22) - (24), the decoupled system may be expressed as

$$\left(\mathbf{a_{0,r}}\mathbf{D}^3 + \mathbf{a_{1,r}}\mathbf{D}^2 + \mathbf{a_{2,r}}\mathbf{D} + \mathbf{a_{3,r}}I\right)\mathbf{F}_{r+1} = \mathbf{R}_{1,r}, \tag{34}$$

$$\left(\mathbf{b_{0,r}}\mathbf{D}^2 + \mathbf{b_{1,r}}\mathbf{D}\right)\boldsymbol{\theta}_{r+1} = \mathbf{R}_{2,r}, \tag{35}$$

$$\left(\mathbf{D}^2 + \mathbf{c_{1,r}}\mathbf{D}\right)\boldsymbol{\phi}_{r+1} = \mathbf{R}_{3,r} \tag{36}$$

where I is an $(N_x+1)\times(N_x+1)$ identity matrix, the bold variable coefficients represent diagonal matrices.
In a more compact form,

$$\begin{aligned}\mathbf{A}_1\mathbf{F}_{r+1} &= R_{1,r},\\ \mathbf{A}_2\boldsymbol{\theta}_{r+1} &= R_{2,r},\\ \mathbf{A}_3\boldsymbol{\phi}_{r+1} &= R_{3,r},\end{aligned} \tag{37}$$

where

$$\begin{aligned}\mathbf{A}_1 &= \mathbf{a_{0,r}}\mathbf{D}^3 + \mathbf{a_{1,r}}\mathbf{D}^2 + \mathbf{a_{2,r}}\mathbf{D} + \mathbf{a_{3,r}}I,\\ \mathbf{A}_2 &= \mathbf{b_{0,r}}\mathbf{D}^2 + \mathbf{b_{1,r}}\mathbf{D},\\ \mathbf{A}_3 &= \mathbf{D}^2 + \mathbf{c_{1,r}}\mathbf{D}.\end{aligned} \tag{38}$$

5 Results and Discussion

In this section, we discuss the significance of the parameters on the velocity, temperature and concentration profiles. The conservation equations are solved using the spectral local linearization method. We found that the outcomes of this problem is similar trend to some previously published works [9], [29], [38].

Figures 2 - 4 show the Casson parameter's effect on the velocity, temperature, and concentration profiles while keeping the other parameters fixed. In figure 2 shows that the velocity profile is decreasing, and as such, the momentum boundary layer thickness increases. Figure 3 shows that increasing the Casson parameter enhances the temperature profile and increases the thermal boundary layer thickness. Figure 4 depicts the concentration profile, which increases with the Casson parameter due to an enhancement in the solutal boundary layer thickness.

Figures 5 - 7 show the effect of velocity ratio parameter on the velocity, temperature, and concentration profiles. From figure 6, we note that the velocity profile decreases when the velocity ratio is less than unity. In comparison, the velocity profile increases when the value of the velocity ratio is greater than unity. This is a similar trend to those obtained in [25]. Figures 6 and 7 show that both temperature and concentration profiles are decreasing when the velocity ratio parameter is increasing.

Figures 8 - 10 illustrate graphs of the velocity, temperature, and concentration profiles when the modified Hartmann number is increased. In figure 8, we note that there is a significant increase in the velocity profiles. The Lorentz force effect is observed when we vary the modified Hartmann number. Generally, the Lorentz force offers resistance to the fluid flow. Here the higher values of the modified Hartmann number lead to a decrease in the Lorentz forces' effect. Thus, an increase in velocity distribution is observed.

Figures 9 and 10 show the effect of modified Hartmann number on temperature and concentration profiles. We can see from the figures that the temperature and the concentration profiles decrease as the modified Hartmann number is increasing. This leads to a decrease in the thermal and solutal boundary layers. The reason behind such behavior is that an increase in the modified Hartmann number amplifies the Lorentz force, which resists the fluid motion. Due to this resistance, a decrease in temperature and solutal distributions are observed.

Figures 11 - 16 portray the impact of appropriate parameters on the entropy generation. The influence of the Reynolds number R_e on the entropy generation number N_G is depicted from figure 11. Entropy generation is an increasing function of R_e. This implies that the enhancement in the entropy production is due to the dominance in the inertial forces, that is, the Reynolds number's higher values. Figure 12 shows that with an increase in the Brinkmann number, entropy generation increases. Higher values of the Brinkmann number indicates higher frictional heating in the system.

Figure 13 depicts that with increasing Casson parameter values, entropy generation decreases. Figure 14 illustrates that entropy generation decreases with the enhancement in modified Hartmann number. An increase in the Hartmann number shows a stronger Lorentz force; this force retards the flow and increases the entropy generation. Figure 15 shows that with the decrease in temperature, entropy generation increases. Entropy is high in regions adjacent to walls. Thus there is a lesser heat transfer in some parts of the sheet due to vanishing temperature gradients. Figure 16 depicts the impact of the dimensionless concentration difference χ. For fixed value of the dimensionless temperature $\Omega = 1$, the entropy generation number N_G increases as χ increases, for a given value of η. This increase is due to the contribution of mass transfer to the entropy generation, and this augmentation continues up to a certain value of η.

We show the impact of the Bejan number on some parameters in Figures 17 - 20. For all parameters considered, we note an opposite trend to the behavior of the entropy generation number. The reason for this is because the Bejan number is a fraction of the heat transfer irreversibility and the total entropy generation number. These profiles' behavior shows that irreversibility due to heat transfer is very dominant and has a high impact on the Bejan number. For higher values of the Brinkmann number and dimensionless concentration, the Bejan number decreases. Although, they coincide after a certain value of the parameters(see Figures 17 and 21). Bejan number escalates with Casson parameter and dimensionless temperature (see Figures 18 and 20). For the modified Hartmann number, a different trend is observed (see Figures 19) up to a certain value of Z, Bejan number increases, and then retards.

5.1 Tables and Figures

Table 1: Comparison of numerical results of $f''(0)$ and $\theta'(0)$ for different values of the velocity ratio parameter when $\delta = Z = Nt = Ec = 0$, $Pr = Le = 1$, $Nb \to 0$ and $\beta \to \infty$.

ϵ	$-f''(0)$		$-\theta'(0)$	
	Present	[28]	Present	[28]
0.10	-0.96939	0.96938	0.60215	0.60281
0.30	-0.84942	0.84942	0.64727	0.64732
0.80	-0.29939	0.29938	0.75709	0.75709
1.00	0.00000	0.00000	0.79787	0.79788
2.00	2.01750	-2.01750	0.97871	0.97872
3.00	4.72928	-4.72928	1.13207	1.13209

Table 2: Variations values of skin friction coefficient, Nusselt, and Sherwood numbers for different values of some parameters when $\delta = Z = 0.5$, $\epsilon = 0.1$, $Pr = 1$, $Nb = 0.3$, $Nt = 0.3$, $Le = 5$; $\beta = 2$, and $Ec = 0.1$.

Z	δ	Nt	ϵ	Ec	β	$\left(1+\frac{1}{\beta}\right) f''(0)$	$-\theta'(0)$	$-\phi'(0)$
0.00						-1.1873	0.4047	1.5307
0.50						-0.8121	0.4572	1.5824
1.00						-0.4639	0.4930	1.6253
	0.10					-0.6134	0.4974	1.6206
	0.20					-0.6783	0.4850	1.6083
	0.40					-0.7757	0.4650	1.5895
		0.10				-0.8121	0.4995	1.6326
		0.30				-0.8121	0.4572	1.5824
		0.50				-0.8121	0.4193	1.5586
			0.00			-0.8411	0.4496	1.5763
			0.30			-0.6844	0.4808	1.6043
			0.80			-0.0512	0.5496	1.6932
				0.00		-0.8121	0.4787	1.5683
				0.10		-0.8121	0.4572	1.5824
				0.50		-0.8121	0.3705	1.6390
					0.10	-2.6539	0.4664	1.6708
					2.00	-0.8121	0.4572	1.5824
					5.00	-0.7097	0.4540	1.5703

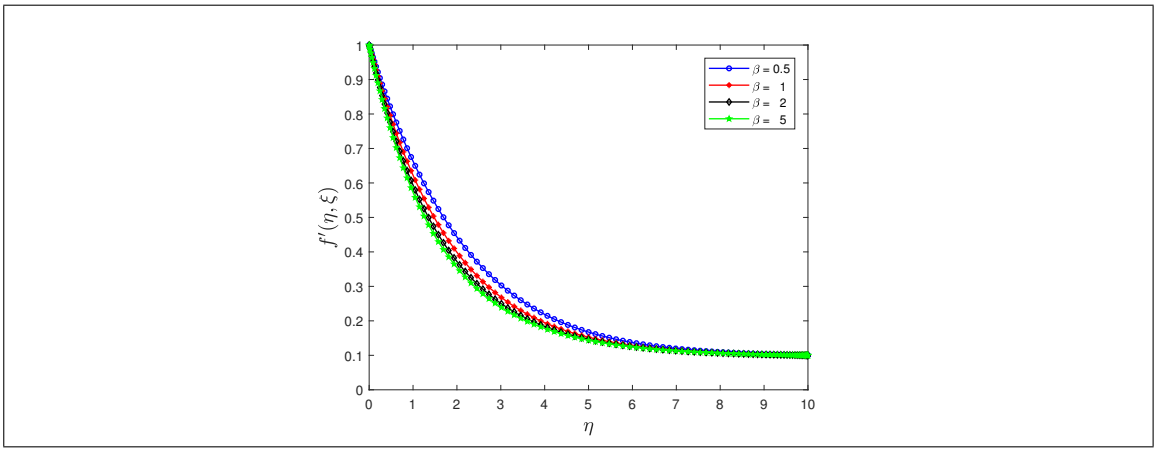

Figure 2: Effect of Casson fluid on the velocity profile when $\delta = Z = 0.5, \epsilon = 0.1, Pr = 1; Nb = Nt = 0.3, Le = 5$ and $Ec = 0.1$.

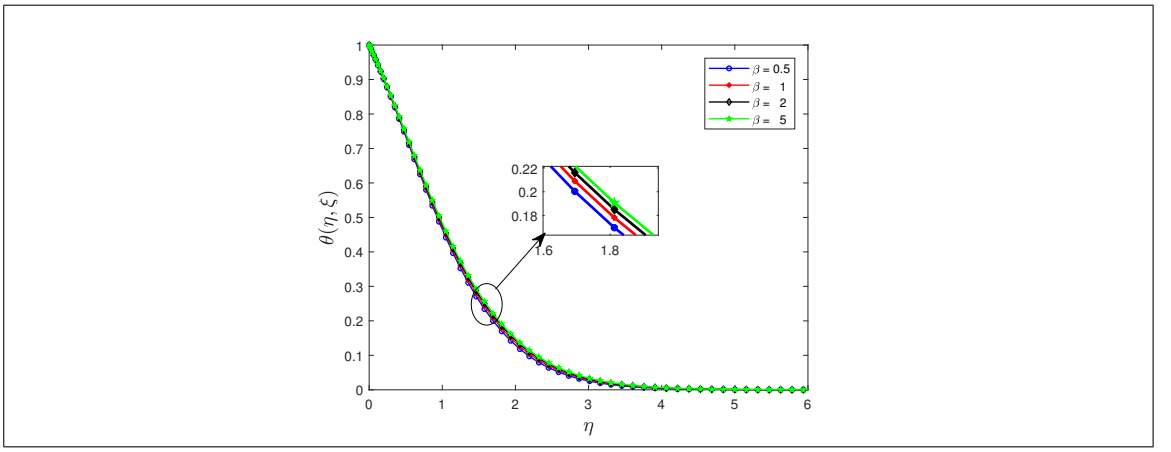

Figure 3: Effect of Casson fluid on the temperature profile when $\delta = Z = 0.5, \epsilon = 0.1, Pr = 1; Nb = Nt = 0.3, Le = 5$ and $Ec = 0.1$.

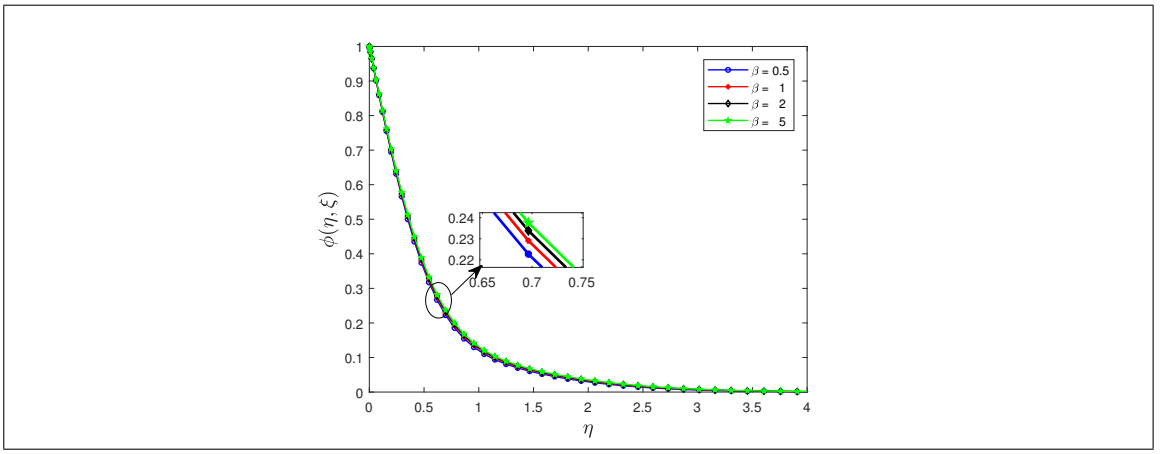

Figure 4: Effect of Casson fluid on the concentration profile when $\delta = Z = 0.5, \epsilon = 0.1, Pr = 1; Nb = Nt = 0.3, Le = 5$ and $Ec = 0.1$.

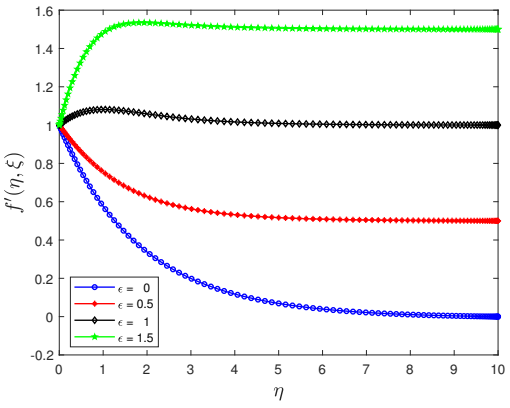

Figure 5: Effect of velocity ratio parameter on the velocity profile when $\beta = 2, \delta = Z = 0.5, Pr = 1; Nb = Nt = 0.3, Le = 5$ and $Ec = 0.1$.

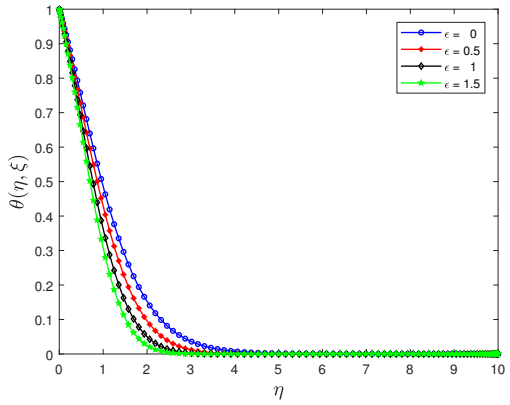

Figure 6: Effect of velocity ratio parameter on the temperature profile when $\beta = 2, \delta = Z = 0.5, Pr = 1; Nb = Nt = 0.3, Le = 5$ and $Ec = 0.1$.

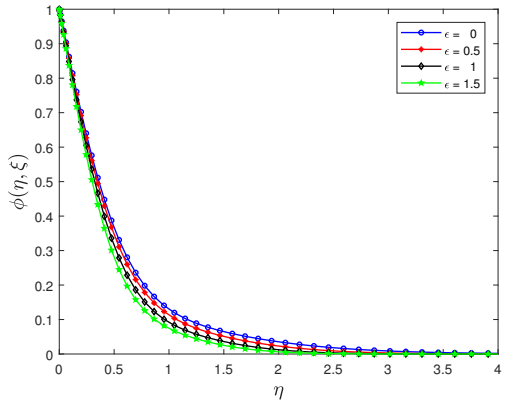

Figure 7: Effect of velocity ratio parameter on the concentration profile when $\beta = 2, \delta = Z = 0.5, Pr = 1; Nb = Nt = 0.3, Le = 5$ and $Ec = 0.1$.

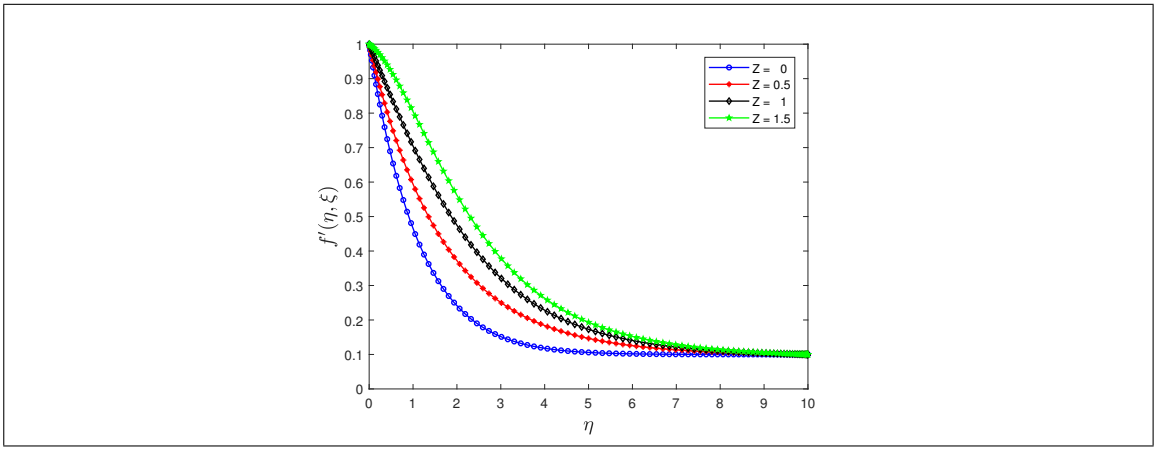

Figure 8: Effect of modified Hartmann number on the velocity profile when $\beta = 2, \delta = 0.5, \epsilon = 0.1, Pr = 1; Nb = Nt = 0.3, Le = 5$ and $Ec = 0.1$.

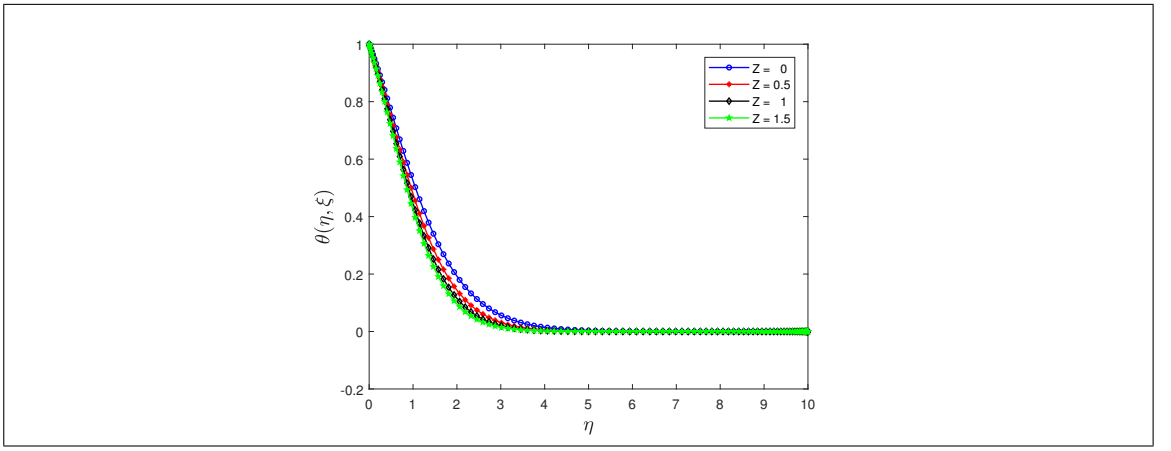

Figure 9: Effect of modified Hartmann number on the temperature profile when $\beta = 2, \delta = 0.5, \epsilon = 0.1, Pr = 1; Nb = Nt = 0.3, Le = 5$ and $Ec = 0.1$.

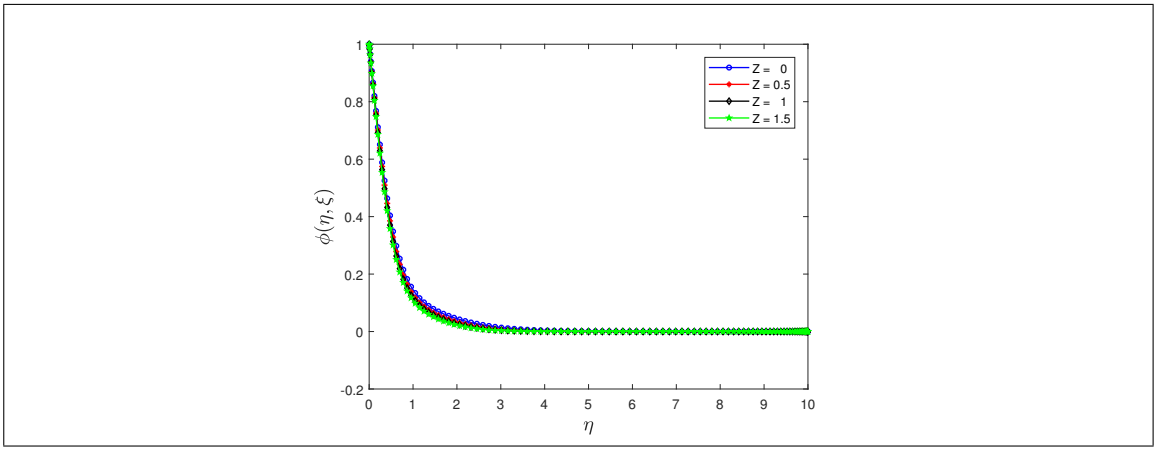

Figure 10: Effect of modified Hartmann number on the concentration profile when $\beta = 2, \delta = 0.5, \epsilon = 0.1, Pr = 1; Nb = Nt = 0.3, Le = 5$ and $Ec = 0.1$.

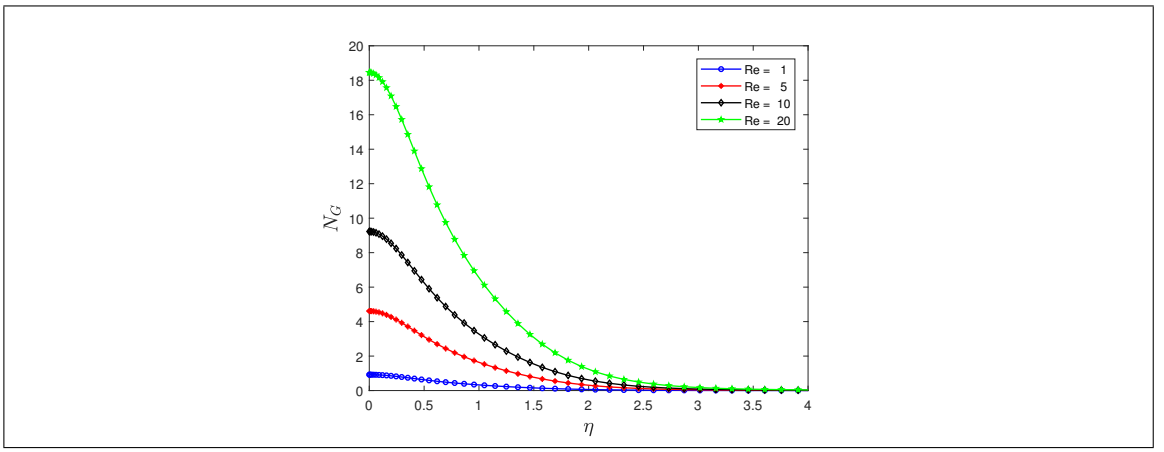

Figure 11: Entropy generation number for different values of the Reynold's number when $Br = 0.5, \Omega = 1$, $Re = 10$, and $\lambda_1 = 0.5$.

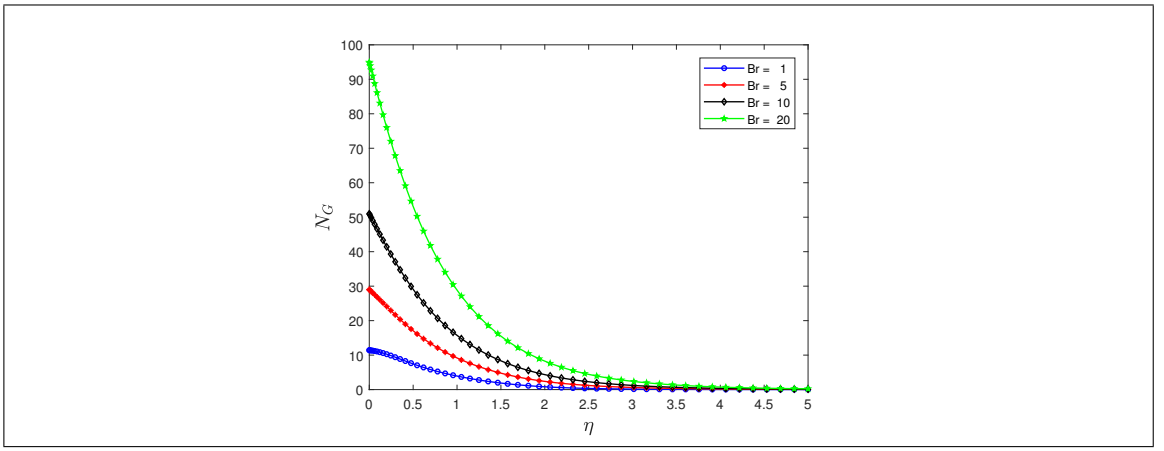

Figure 12: Entropy generation number for different values of the Brinkmann number when $Br = 0.5, \Omega = 1$, $Re = 10$, and $\lambda_1 = 0.5$.

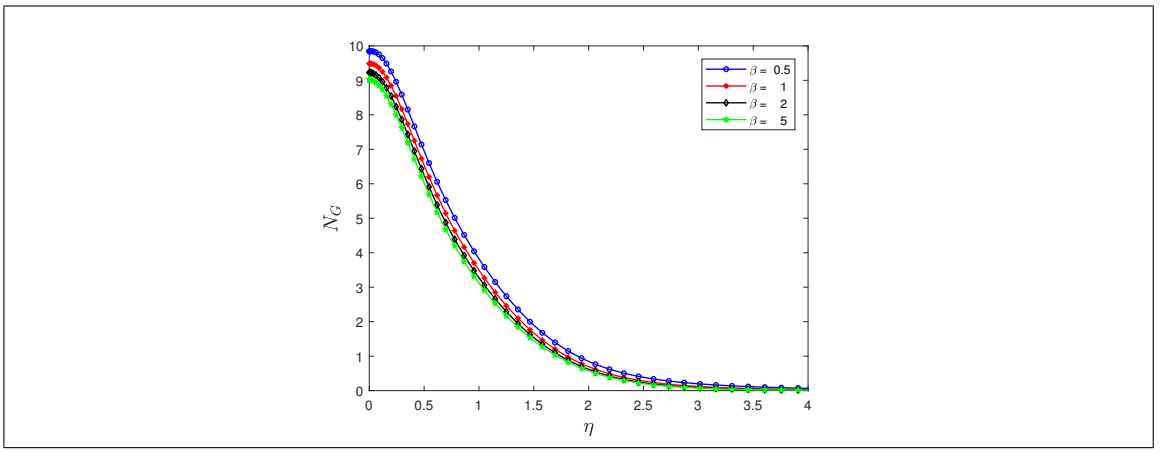

Figure 13: Entropy generation number for different values of the Casson parameter when $Br = 0.5, \Omega = 1$, $Re = 10$, and $\lambda_1 = 0.5$.

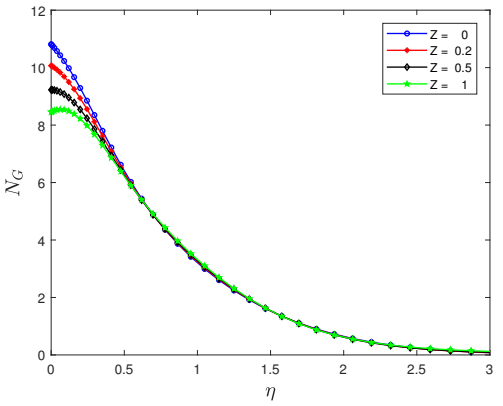

Figure 14: Entropy generation number for different values of the modified Hartmann number when $Br = 0.5, \Omega = 1, Re = 10$, and $\lambda_1 = 0.5$.

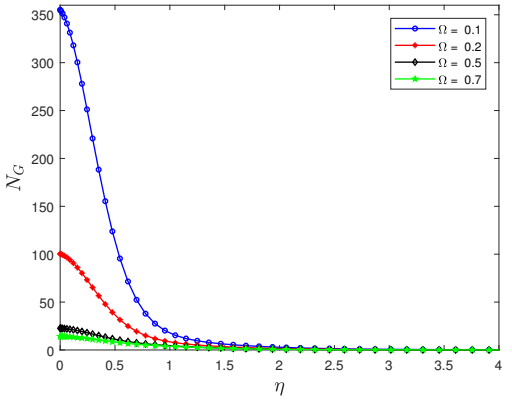

Figure 15: Entropy generation number for different values of the dimensionless temperature when $Br = 0.5, \Omega = 1, Re = 10$, and $\lambda_1 = 0.5$.

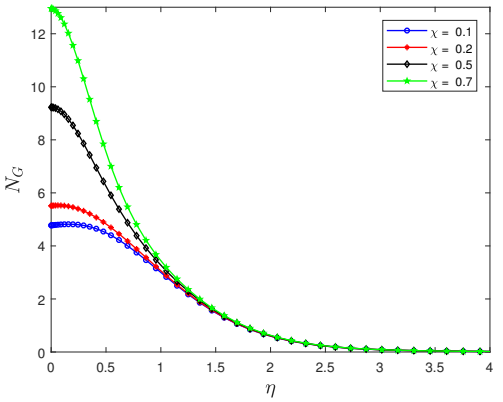

Figure 16: Entropy generation number for different values of the dimensionless concentration when $Br = 0.5, \Omega = 1, Re = 10$, and $\lambda_1 = 0.5$.

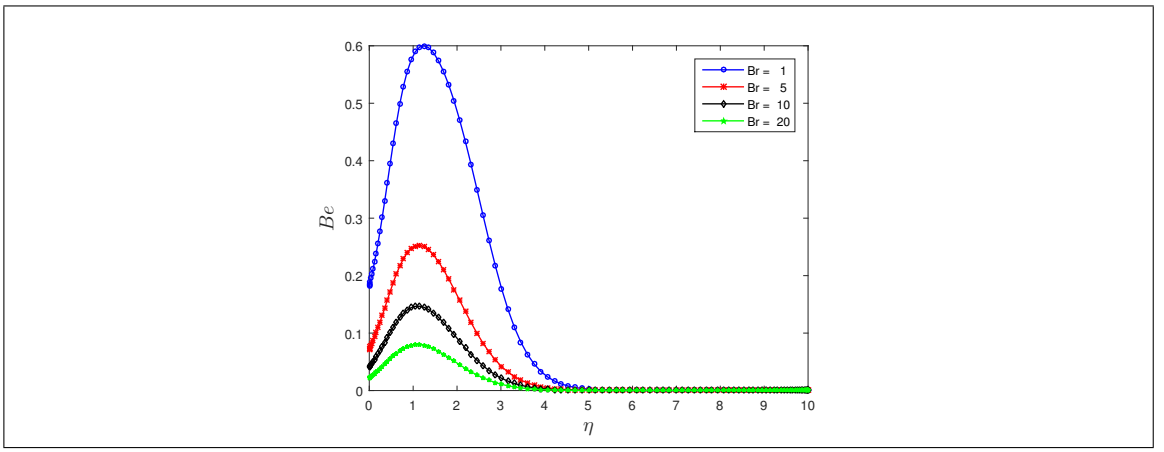

Figure 17: Bejan number for different values of the Brinkmann number.

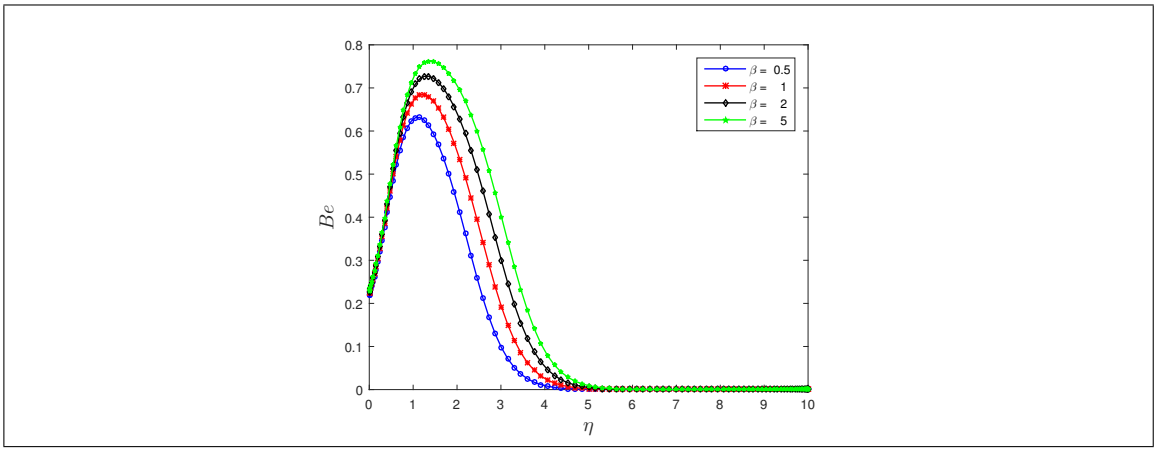

Figure 18: Bejan number for different values of the Casson parameter.

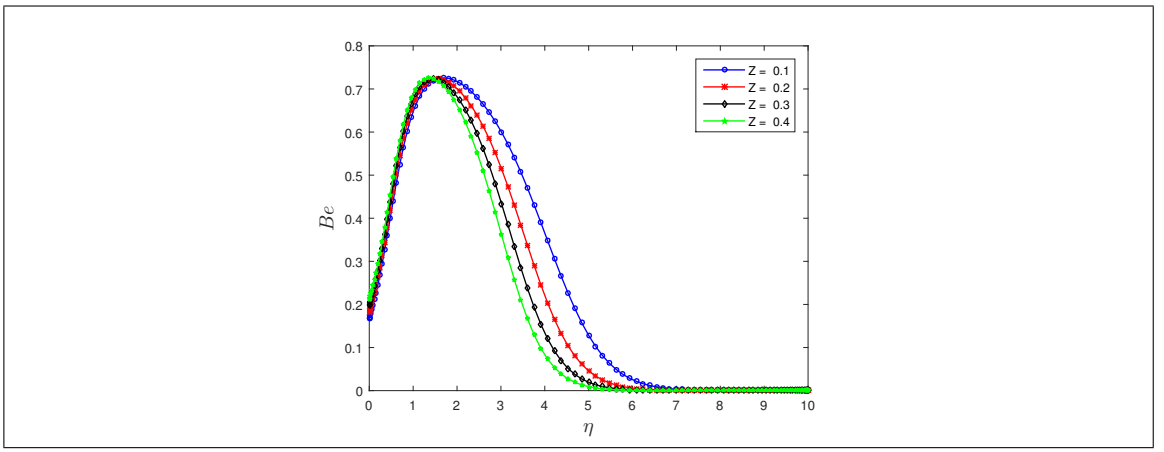

Figure 19: Bejan number for different values of the modified Hartmann number.

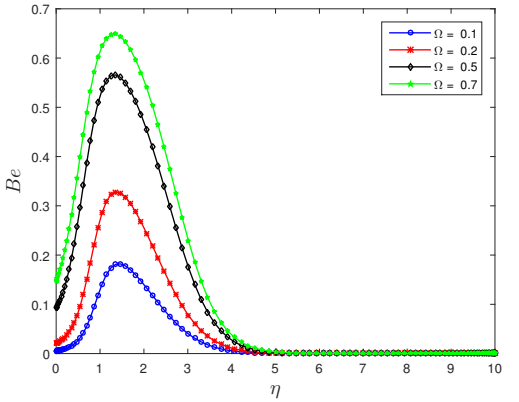

Figure 20: Bejan number for different values of the dimensionless temperature.

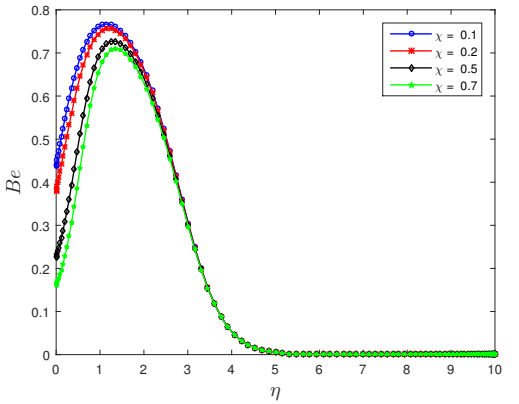

Figure 21: Bejan number for different values of the dimensionless concentration.

6 Conclusions

We have analyzed the flow heat and mass transfer of a Casson nanofluid past an electromagnetic stretching Riga plate. The problem considers the effect of entropy generation, viscous dissipation, Brownian motion, and thermophoresis diffusion. The results obtained in the study are summarized as follows:

- Velocity profile decreases with the increase in Casson parameter, while it increases for increasing values of the modified Hartmann number.
- Velocity profile increases when the velocity ratio parameter is less than unity, whereas it decreases for the velocity ratio parameter values greater than unity.
- Temperature and concentration profiles increase with an increase in the Casson parameter, whereas the profiles decrease when the velocity ratio parameter and Modified Hartmann number are increased.
- Entropy generation increases with the increase in Brinkmann number.
- Increasing modified Hartmann number leads to a decrease in entropy generation.
- Entropy generation increases with an increase in the value of the dimensionless concentration.

Acknowledgement Authors are thankful to the Amity University, Kolkata-700135, West Bengal, India for the necessary support. Also, authors are grateful to the editor of this journal for giving their kind suggestions on this paper.

Conflicts of Interest The authors state that they do not have a conflict of interest.

References

[1] T. Abbas, M. Ayub, M. Bhatti, M. Rashidi & M. Ali (2016). Entropy generation on nanofluid flow through a horizontal Riga plate. *Entropy*, *18*(6), 223. https://doi.org/10.3390/e18060223.

[2] M. H. Abolbashari, N. Freidoonimehr, F. Nazari & M. M. Rashidi (2015). Analytical modeling of entropy generation for Casson nano-fluid flow induced by a stretching surface. *Advanced Powder Technology*, *26*(2), 542–552. https://doi.org/10.1016/j.apt.2015.01.003.

[3] A. Ahmad, S. Asghar & S. Afzal (2016). Flow of nanofluid past a Riga plate. *Journal of Magnetism and Magnetic Materials*, *402*, 44–48. https://doi.org/10.1016/j.jmmm.2015.11.043.

[4] R. Ahmad, M. Mustafa & M. Turkyilmazoglu (2017). Buoyancy effects on nanofluid flow past a convectively heated vertical Riga-plate: A numerical study. *International Journal of Heat and Mass Transfer*, *111*, 827–835. https://doi.org/10.1016/j.ijheatmasstransfer.2017.04.046.

[5] M. Atlas, S. Hussain & M. Sagheer (2018). Entropy generation and squeezing flow past a Riga plate with Cattaneo-Christov heat flux. *Bulletin of the Polish Academy of Sciences: Technical Sciences*, *66*(3), 291–300. https://10.24425/123435.

[6] J. Buongiorno (2006). Convective transport in nanofluids. *Journal of Heat Transfer*, *128*, 240–250. https://doi.org/10.1115/1.2150834.

[7] C. Canuto, M. Y. Hussaini, A. Quarteroni & T. A. Zhang (1988). *Spectral methods in fluid dynamics*. Springer, Berlin, Heidelberg.

[8] S. Choi (1995). Ehnancing thermal conductivity of fluids with nanoparticles. *ASME*, *231*, 99–106.

[9] M. Das, G. Mahanta & S. Shaw (2020). Heat and mass transfer effect on an unsteady MHD radiative chemically reactive Casson fluid over a stretching sheet in porous medium. *Heat Transfer*, *49*(8), 4350–4369. https://doi.org/10.1002/htj.21830.

[10] S. K. Das, S. U. S. Choi & H. E. Patel (2006). Heat transfer in nanofluids - A review. *Heat Transfer Engineering*, *27*(10), 3–19.

[11] R. Dash, K. Mehta & G. Jayaraman (1996). Casson fluid flow in a pipe filled with a homogeneous porous medium. *International Journal of Engineering Science*, *34*(10), 1145–1156.

[12] A. Gailitis & O. Lielausis (1961). On the possibility to reduce the hydrodynamic resistance of a plate in aelectro-lyte. *Applied Magnetohydrodynamics*, *12*, 143–146.

[13] Y. Gupta, P. Rana, O. Beg & A. Kadir (2020). Multiple solutions for slip effects on dissipative magneto-nanofluid transport phenomena in porous media: Stability analysis. *Journal of Applied and Computational Mechanics*, *6*(4), 956–967. https://10.22055/jacm.2019.30144.1689.

[14] A. Hakeem, P. Ragupathi, S. Saranya & B. Ganga (2020). Three dimensional non-linear radiative nanofluid flow over a Riga plate. *Journal of Applied and Computational Mechanics*, *6*(4), 1012–1029. https://10.22055/jacm.2019.30095.1678.

[15] M. Hamad (2011). Analytical solution of natural convection flow of a nanofluid over a linearly stretching sheet in the presence of magnetic field. *International Communications in Heat and Mass Transfer*, *38*(4), 487–492.

[16] T. Hayat, T. Abbas, M. Ayub, M. Farooq & A. Alsaedi (2016). Flow of nanofluid due to convectively heated Riga plate with variable thickness. *Journal of Molecular Liquids*, *222*, 854–862. https://doi.org/10.1016/j.molliq.2016.07.111.

[17] T. Hussain, S. Shehzad, A. Alsaedi, T. Hayat & M. Ramzan (2015). Flow of casson nanofluid with viscous dissipation and convective conditions- A mathematical model. *Journal of Central South University*, *22*, 1132–1140.

[18] W. Khan & I. Pop (2010). Boundary layer flow of a nanofluid past a stretching sheet. *International Journal of Heat and Mass Transfer*, *53*(11-12), 2477–2483.

[19] A. Kumar, R. Tripathi, R. Singh & M. Sheremet (2021). Entropy generation on double diffusive MHD Casson nanofluid flow with convective heat transfer and activation energy. *Indian Journal of Physics*, *95*, 1423–1436.

[20] A. Kunetsov & D. Nield (2014). Natural convective boundary layer flow of a nanofluid past a vertical plate: A revised model. *International Journal of Thermal Sciences*, *77*, 126–129.

[21] G. Makanda, S. Shaw & P. Sibanda (2015). Diffusion of chemically reactive species in Casson fluid flow over an unsteady stretching surface in porous medium in the presence of a magnetic field. *Mathematical Problems in Engineering*, *2015*, Article ID:724596. https://doi.org/10.1155/2015/724596.

[22] O. Makinde & A. Aziz (2011). Boundary layer flow of a nanofluid past a stretching sheet with a convective boundary condition. *International Journal of Thermal Sciences*, *50*(7), 1326–1332.

[23] S. S. Motsa (2013). A new spectral local linearization method for nonlinear boundary layer flow problems. *Journal of Applied Mathematics*, *2013*, Article ID: 423628. http://dx.doi.org/10.1155/2013/423628.

[24] S. Motsa, Z. Makukula & S. Shateyi (2013). Spectral local linearisation approach for natural convection boundary layer flow. *Mathematical Problems in Engineering*, *2013*, Article ID: 765013. https://doi.org/10.1155/2013/765013.

[25] T. Motsumi & O. Makinde (2012). Effects of thermal radiation and viscous dissipation on boundary layer flow of nanofluids over a permeable moving flat plate. *Physica Scripta*, *86*(4), 045003. https://doi.org/10.1088/0031-8949/86/04/045003.

[26] S. Mukhopadhyay, P. De, K. Bhattacharyya & G. Layek (2013). Casson fluid flow over an unsteady stretching surface. *Ain Shams Engineering Journal*, *4*(4), 933–938.

[27] M. Mustafa & J. A. Khan (2015). Model for flow of Casson nanofluid past a non-linearly stretching sheet considering magnetic field effects. *AIP Advances*, *5*(7), 077148. https://doi.org/10.1063/1.4927449.

[28] S. Nadeem, R. Mehmood & S. Motsa (2015). Numerical investigation on MHD oblique flow of Walter's B type nano fluid over a convective surface. *International Journal of Thermal Sciences*, *92*, 162–172. https://doi.org/10.1016/j.ijthermalsci.2015.01.034.

[29] M. Nayak, J. Prakash, D. Tripathi, V. Pandey, S. Shaw & O. Makinde (2020). 3D bioconvective multiple slip flow of chemically reactive Casson nanofluid with gyrotactic microorganisms. *Heat Transfer*, *49*(1), 135–153. https://doi.org/10.1002/htj.21603.

[30] A. Noghrehabadi, R. Pourrajab & M. Ghalambaz (2012). Effect of partial slip boundary condition on the flow and heat transfer of nanofluids past stretching sheet prescribed constant wall temperature. *International Journal of Thermal Sciences*, *54*, 253–261.

[31] I. Oyelakin & P. Sibanda (2020). A numerical study of entropy generation in radiative Casson nanofluid flow. *Engineering Reports*, *2*(11), e12257. https://doi.org/10.1002/eng2.12257.

[32] I. Oyelakin, S. Mondal & P. Sibanda (2016). Unsteady Casson nanofluid flow over a stretching sheet with thermal radition, convective and slip boundary condition. *Alexandria Engineering Journal*, *55*(2), 1025–1035.

[33] J. Qing, M. M. Bhatti, M. A. Abbas, M. M. Rashidi & M. E.-S. Ali (2016). Entropy generation on MHD Casson nanofluid flow over a porous stretching/shrinking surface. *Entropy*, *18*(4), 123. https://doi.org/10.3390/e18040123.

[34] C. Raju, N. Sandeep, V. Sungunamma, M. Babu & J. Reddy (2016). Heat and mass transfer in magnetohydrodynamic Casson fluid over an exponentially permeable stretching surface. *Engineering Science and Technology, an International Journal*, *19*(1), 45–52.

[35] C. RamReddy & V. Chukka (2017). Bivariate pseudo-spectral local linearisation method for mixed convective flow over the vertical frustum of a cone in a nanofluid with soret and viscous dissipation effects. *Journal of Mechanics*, *33*(5), 687–702.

[36] H. Sayehvand & A. B. Parsa (2017). A new numerical method for investigation of thermophoresis and Brownian motion effects on MHD nanofluid flow and heat transfer between parallel plates partially filled with a porous medium. *Results in Physics*, *7*, 1595–1607. https://doi.org/10.1016/j.rinp.2017.02.004.

[37] S. Shateyi & G. Marewo (2014). Numerical analysis of MHD stagnation point flow of Casson fluid, heat and mass transfer over a stretching sheet. In *International Conference on Finite Differences, Finite Elements, Finite Volumes, Boundary Elements*, pp. 128–132. Gdansk.

[38] S. Shaw, G. Mahanta & M. Das (2019). Thermal and solutal Marangoni stagnation point Casson fluid flow over a stretching sheet in the presence of radiation, Soret and Dofour effect with chemical reaction. *Heat Transfer*, *48*(1), 323–342. https://doi.org/10.1002/htj.21386.

[39] H. M. Sithole, S. Mondal, P. Sibanda & S. S. Motsa (2017). An unsteady MHD Maxwell nanofluid flow with convective boundary conditions using spectral local linearization method. *Open Physics*, *15*(1), 637–646. https://doi.org/10.1515/phys-2017-0074.

[40] L. N. Trefethen (2000). *Spectral methods in MATLAB*. SIAM, Philadelphia.